

Complementary Frequency-Varying Awareness Network for Open-Set Fine-Grained Image Recognition

Jiayin Sun, Hong Wang and Qiulei Dong

Abstract—Open-set image recognition is a challenging topic in computer vision. Most of the existing works in literature focus on learning more discriminative features from the input images, however, they are usually insensitive to the high- or low-frequency components in features, resulting in a decreasing performance on fine-grained image recognition. To address this problem, we propose a Complementary Frequency-varying Awareness Network that could better capture both high-frequency and low-frequency information, called CFAN. The proposed CFAN consists of three sequential modules: (i) a feature extraction module is introduced for learning preliminary features from the input images; (ii) a frequency-varying filtering module is designed to separate out both high- and low-frequency components from the preliminary features in the frequency domain via a frequency-adjustable filter; (iii) a complementary temporal aggregation module is designed for aggregating the high- and low-frequency components via two Long Short-Term Memory networks into discriminative features. Based on CFAN, we further propose an open-set fine-grained image recognition method, called CFAN-OSFGR, which learns image features via CFAN and classifies them via a linear classifier. Experimental results on 3 fine-grained datasets and 2 coarse-grained datasets demonstrate that CFAN-OSFGR performs significantly better than 9 state-of-the-art methods in most cases.

I. INTRODUCTION

Open-set image recognition (OSR) has received more and more attention recently, which aims to both classify known-class images and identify unknown-class images. Existing OSR methods [1–21] could be roughly divided into two categories: CNN (Convolutional Neural Network)-based methods and transformer-based methods. Both the two categories of OSR methods have demonstrated their effectiveness to some extent on coarse-grained datasets. However, as shown in [22, 23], their performance would decrease in open-set fine-grained image recognition task (OSFGR), which is a sub-task of OSR where the differences among object classes become subtle. Thus in this paper, we focus on OSFGR.

As indicated in [24–27], many existing CNN/transformer-based closed-set classification methods could not effectively

TABLE I: OSFGR results on high/low-frequency images (HFI/LFI) from Aircraft by ResNet50/SwinB backbone models and our proposed CFAN-OSFGR based on ResNet50/SwinB backbones.

Model	Images	ACC	AUROC (Easy/Medium/Hard)	OSCR (Easy/Medium/Hard)
ResNet50	HFI	0.729	0.705/0.668/0.510	0.589/0.552/0.537
	LFI	0.645	0.601/0.524/0.458	0.564/0.432/0.378
SwinB	HFI	0.794	0.789/0.726/0.655	0.712/0.681/0.603
	LFI	0.836	0.818/0.782/0.699	0.753/0.722/0.638
ours (ResNet50)	HFI	0.743	0.736/0.691/0.608	0.624/0.607/0.596
	LFI	0.718	0.685/0.601/0.599	0.643/0.562/0.526
ours (SwinB)	HFI	0.834	0.826/0.772/0.723	0.755/0.728/0.671
	LFI	0.867	0.844/0.812/0.770	0.785/0.762/0.689

capture either high-frequency or low-frequency information from coarse-grained images: Specifically, CNN-based OSR methods are generally insensitive to low-frequency components, while transformer-based OSR methods are generally insensitive to high-frequency components. Furthermore, as done for classifying closed-set coarse-grained images in [25], we evaluate a typical CNN (ResNet50) and a typical transformer (SwinB) on high-frequency images (called HFI) and low-frequency images (called LFI) generated from a fine-grained dataset Aircraft [28] under the same open-set setting as [23], and the corresponding AUROC and OSCR (the two metrics are defined in Sec. IV-A) under three difficulty modes (*i.e.*, Easy/Medium/Hard) are reported in Table I. As seen from this table, ResNet50 performs better on HFI than on LFI while SwinB performs better on LFI than HFI, demonstrating that they have to be confronted with the same problem in OSFGR as that in closed-set classification. Naturally, the following question is raised: “How to capture both high-frequency and low-frequency information from fine-grained images more effectively for open-set recognition?”

To address this question, we propose a Complementary Frequency-varying Awareness Network (called CFAN) for better capturing both high- and low-frequency information. CFAN consists of three sequential modules: a feature extraction module, a frequency-varying filtering module, and a complementary temporal aggregation module. The feature extraction module, which could be an arbitrary feature extractor in literature (*e.g.*, ResNet [29], and SwinB [30]), is firstly used to extract the preliminary features from the input fine-grained images. Then, the frequency-varying filtering module is designed to decompose the extracted preliminary features into both high- and low-frequency components in the

The corresponding author is Qiulei Dong.

Jiayin Sun and Qiulei Dong are with the National Laboratory of Pattern Recognition, Institute of Automation, Chinese Academy of Sciences, Beijing 100190, China, the School of Artificial Intelligence, University of Chinese Academy of Sciences, Beijing 100049, China, and the Center for Excellence in Brain Science and Intelligence Technology, Chinese Academy of Sciences, Beijing 100190, China (e-mail: jiayin.sun@nlpr.ia.ac.cn; ql-dong@nlpr.ia.ac.cn).

Hong Wang is with the College of Life Science, University of Chinese Academy of Sciences, Beijing 100049, China (email: Chinah-wang@ucas.ac.cn)

frequency domain via an explored frequency-adjustable filter. Finally, the complementary temporal aggregation module is explored to aggregate the high- and low-frequency feature components learnt from the frequency-varying filtering module via two LSTMs (Long Short-Term Memory Networks) into discriminative features, inspired by the ability of LSTMs for modeling time-series data in many other visual tasks [31–34]. Furthermore, we explore a CFAN-based method to handle the OSFGR task, called CFAN-OSFGR, where the proposed CFAN is used to extract fine-grained image features and then a linear classifier is employed to classify these features.

The main contributions of this paper are summarized as:

(1) We explore the frequency-varying filtering module which could separate out high- and low-frequency components from an image feature via a designed frequency-adjustable filter. The designed filter could flexibly switch from a high-pass (also low-pass) filter to a full-pass filter in the frequency domain. Moreover, we explore the complementary temporal aggregation module, which could effectively aggregate multi-band high- and low-frequency feature components.

(2) We propose the CFAN, which integrates the two explored modules for learning features that could better capture the high- and low-frequency information from the fine-grained images. The proposed CFAN could be used as a stronger feature extractor in both the coarse-grained and fine-grained image recognition tasks.

(3) We propose the CFAN-OSFGR method for handling the OSFGR task by integrating the CFAN with a linear classifier, whose priority to 9 state-of-the-art methods have been demonstrated in Sec. IV

II. RELATED WORKS

Here, we briefly review the CNN-based and transformer-based OSR/OSFGR methods in literature, and some typical works that enhance features in the frequency domain.

A. OSR/OSFGR Methods

CNN-based Methods. Most existing OSR/OSFGR methods are CNN-based methods, most of which are evaluated on coarse-grained datasets. Zhang *et al.* [8] adopted a resflow-net [35] to model the known-class likelihood scores and used the latent features for classification. Kong and Ramanan [17] adversarially trained a VGG [36] feature extractor against a discriminator for distinguishing known-class samples from outliers. Chen *et al.* [14] mined unknown-class features in the extra-class space of each known class via a ResNet [29], then trained the model with known-class samples and these features adversarially for encouraging the known-class feature space to be more compact. Yang *et al.* [13] modeled the feature distribution of each known class as a Gaussian mixture for learning more discriminative features via a ResNet by prototype learning. Cao *et al.* [10] used a VGG-based GMVAE [37] for modeling such distributions. Besides, a few OSFGR methods [22, 23] have been proposed, aiming to learn more discriminative features. Dai *et al.* [22] analyzed the characteristics of different classification scores and chose the class activation mapping values outputted from a VGG for

preserving fine-grained information. Vaze *et al.* [23] proposed to take full advantage of multiple training strategies for improving the discriminability of known-class features extracted from a ResNet backbone.

Transformer-based Methods. Inspired by the success of vision transformers in closed-set image recognition tasks [30, 38–40], a few transformer-based methods [20, 21] have been proposed. Sun *et al.* [21] introduced multiple mixtures of exponential power distributions into a transformer-based autoencoder for modeling the distributions of known-class features. Azizmalayeri and Rohban [20] integrated various data augmentation strategies for learning more generalized feature representations via a transformer.

B. Frequency Based Feature Enhancement

Recently, some frequency-based feature enhancement works have been proposed in other visual task [41–43]. Rao *et al.* [41] proposed a global filter network for learning long-term spatial dependencies in an image, they used learnable filters at different layers and encouraged each filter to pass frequency component at an appropriate band. Liu *et al.* [42] proposed a global spectral filter memory network, aiming to learn long-term spatial dependencies between different video frames, and they used the traditional Gaussian filter for frequency filtering. Qin *et al.* [43] proposed a multi-spectral channel attention, which used the conventional global average pooling operation instead of frequency filters for feature decomposition in the frequency domain. Different from these methods, CFAN-OSFGR uses an adjustable frequency filter which can obtain a set of high- and low-frequency components at various frequency bands by adjusting the adjustable vectors, aiming to make use of more abundant frequency information.

III. COMPLEMENTARY FREQUENCY-VARYING AWARENESS NETWORK FOR OSFGR

A. Complementary Frequency-Varying Awareness Network

Here, we propose the Complementary Frequency-varying Awareness Network (CFAN), consisting of a feature extraction module, a frequency-varying filtering module, and a complementary temporal aggregation module. Firstly, we introduce the whole architecture of CFAN and the feature extraction module. Then, we describe the other two modules in the proposed CFAN in detail.

3.1.1 Architecture and Feature Extraction Module

As seen from Fig. 1, CFAN takes object images as its inputs, and aims to output discriminative features. It contains three sequential modules, a feature extraction module, a frequency-varying filtering (FVF) module, and a complementary temporal aggregation (CTA) module. The feature extraction module is firstly used to learn preliminary features from the input images. Once the preliminary features have been learnt from the feature extraction module, the FVF module is used for converting the preliminary features into time-series features that cover various high- and low-frequency bands. Finally, the CTA module is used for aggregating the high- and low-frequency components into discriminative features.

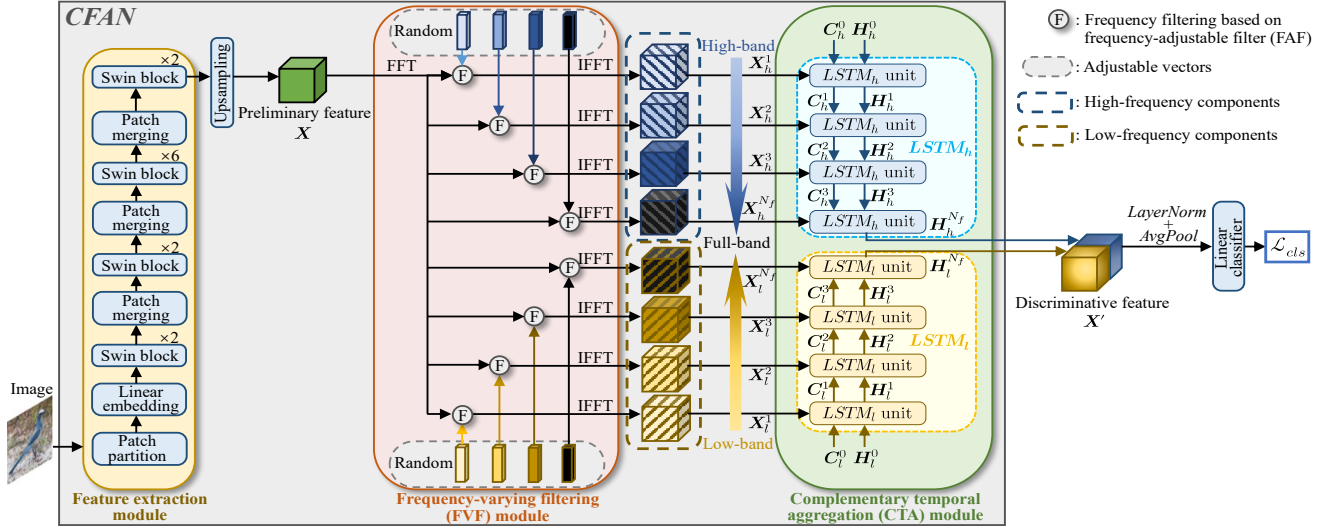


Fig. 1: Architecture of the proposed CFAN-OSFGR method: Firstly, an image is fed into the proposed CFAN for obtaining a corresponding discriminative feature X' , which consists of three sequential modules, including a feature extraction module (ResNet50 [29] and SwinB [30] are respectively used here, and we show the SwinB as an example) for extracting a preliminary image feature X , a frequency-varying filtering module for separating out the high- and the low-frequency components from the preliminary feature in the frequency domain, and a complementary temporal aggregation module for aggregating the high- and the low-frequency feature components into a discriminative feature. Then, the discriminative feature is fed into a linear classifier. CFAN-OSFGR is trained by minimizing the classification loss \mathcal{L}_{cls} .

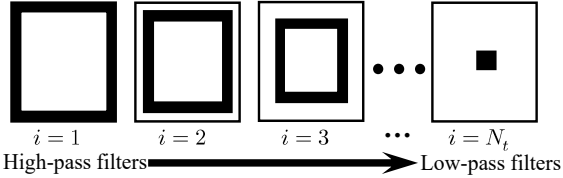


Fig. 2: Sketch of the sequence of band-pass template filters $\{\mathbf{T}_i\}_{i=1}^{N_t}$ at each channel in the frequency-varying filtering module. Each value in these filters is either 1 (in black) or 0 (in white).

It has to be pointed out that many feature extractors in literature (e.g., VGG [36], ResNet [29], SwinB [30], etc.) could be straightforwardly used as the feature extraction module. Here, we simply use ResNet50 [29] and SwinB [30] (as shown in the left-most yellow box in Fig. 1) as the feature extraction module, respectively. The FVF module and the CTA module would be described in detail in the following subsections.

3.1.2 Frequency-Varying Filtering Module

The FVF module is designed for separating out both high- and low-frequency components from the preliminary features in the frequency domain via an explored frequency-adjustable filter. As shown in the red box in Fig. 1, this module takes the preliminary feature extracted from each input image by the feature extraction module as its input, and outputs two time series of feature components at various high and low frequencies respectively.

Frequency-Adjustable Filter. In order to extract various bands of high- and low-frequency information flexibly, we design the frequency-adjustable filter, which is a weighted combination of a sequence of N_t (here we set $N_t = 20$) band-pass template filters $\{\mathbf{T}_i\}_{i=1}^{N_t}$ as shown in Fig. 2. This filter

has a high-pass form F_h and a low-pass form F_l as:

$$F_h = \sum_{i=1}^{N_t} f_i^h \mathbf{T}_i, \quad F_l = \sum_{i=1}^{N_t} f_i^l \mathbf{T}_i \quad (1)$$

where $\{f_i^h\}_{i=1}^{N_t}$ (also $\{f_i^l\}_{i=1}^{N_t}$) is a set of weighting coefficients. Here, we use the exponential power (EP) function values to assign these coefficients, considering that the EP function is a member of the function family whose function shape can be flexibly adjusted as indicated in [44–46]. According to the parametric form suggested in [44], the complete form of the EP function is formulated as:

$$EP(\mathbf{m}) = \frac{1}{2\sigma p^{\frac{1}{p}} \Gamma(1 + \frac{1}{p})} e^{-\frac{|\mathbf{m} - \mu|^p}{p\sigma^p}} \quad (2)$$

where \mathbf{m} is the independent variable, $\Gamma(\cdot)$ is the Gamma function, and $\{\mu, \sigma, p\}$ ($\sigma > 0, p > 0$) is a group of parameters that control the position, scale, and shape of the EP function respectively. It is noted that the shape parameter p plays a leading role in controlling the shape of the EP function, hence, we use p as an adjustable vector to switch the shape of the EP function from steep to gentle, which switches the frequency filter whose coefficients are assigned by the EP function values from a high- or low-pass filter to a full-pass filter. In order to limit the function values within $(0, 1)$, we discard the coefficient part before the exponential power part of this formula. It is noted that the EP function is axial-symmetrical to the axis $\mathbf{m} = \mu$, hence, the sequence of weighting coefficients $\{f_i^h\}_{i=1}^{N_t}$ for the high-pass filter F_h and the sequence of weighting coefficients $\{f_i^l\}_{i=1}^{N_t}$ for the low-pass filter F_l can be obtained by simply setting the axis of symmetry at $\mathbf{m} = \mathbf{0}$ and $\mathbf{m} = N_t \cdot \mathbf{I}$ (where \mathbf{I} is a vector with all values being 1) respectively and taking the EP func-

tion values corresponding to the evenly-spaced independent variable values which are sampled over the interval $(0, N_t \cdot \mathbf{I})$ (here we sample $\mathbf{m} = 0.5 \cdot \mathbf{I}, 1.5 \cdot \mathbf{I}, \dots, (N_t - 0.5) \cdot \mathbf{I}$) as the weighting coefficients for the template filters. Thus, the i -th elements ($i \in \{1, 2, \dots, N_t\}$) \mathbf{f}_i^h and \mathbf{f}_i^l in the two sequences $\{\mathbf{f}_i^h\}_{i=1}^{N_t}$ and $\{\mathbf{f}_i^l\}_{i=1}^{N_t}$ can be formulated as:

$$\mathbf{f}_i^h = e^{-\frac{|\mathbf{m}-0|\mathbf{p}_h}{\mathbf{p}_h \sigma \mathbf{p}_h}}, \quad \mathbf{f}_i^l = e^{-\frac{|\mathbf{m}-N_t \cdot \mathbf{I}|\mathbf{p}_l}{\mathbf{p}_l \sigma \mathbf{p}_l}} \quad (3)$$

s.t. $\mathbf{m} = (i - 0.5) \cdot \mathbf{I}, \quad \sigma = N_t \cdot \mathbf{I}$

where the values in the two adjustable vectors \mathbf{p}_h and \mathbf{p}_l are separately adjusted varying in $[p_{min}, p_{max}]$, where p_{min} and p_{max} are two preset constants. The high-pass filter \mathbf{F}_h (or the low-pass filter \mathbf{F}_l) inclines to high-pass filtering (or low-pass filtering) when the values in \mathbf{p}_h (or \mathbf{p}_l) get closer to p_{min} , and inclines to full-pass filtering when the values get closer to p_{max} .

Frequency Filtering Process. Here, we describe the filtering process in the FVF module. Firstly, we conduct the Fast Fourier Transform (FFT) at each channel on the preliminary feature map \mathbf{X} with N_c channels: $\mathbf{Z} = \mathcal{F}(\mathbf{X})$, and centralize the complex spectrum \mathbf{Z} . Next, a time series of high-frequency components $\{\mathbf{Z}_h^t\}_{t=1}^{N_f}$ and a time series of low-frequency components $\{\mathbf{Z}_l^t\}_{t=1}^{N_f}$ can be obtained from \mathbf{Z} by a time series of high-pass filters $\{\mathbf{F}_h^t\}_{t=1}^{N_f}$ and a time series of low-pass filters $\{\mathbf{F}_l^t\}_{t=1}^{N_f}$ by utilizing the designed frequency-adjustable filter, whose t -th elements ($t \in \{1, 2, \dots, N_f\}$) can be formulated as:

$$\mathbf{Z}_h^t = \mathbf{Z} \odot \mathbf{F}_h^t, \quad \mathbf{Z}_l^t = \mathbf{Z} \odot \mathbf{F}_l^t \quad (4)$$

where ‘ \odot ’ represents the element-wise product operator; N_f is the length of the time series. $\{\mathbf{F}_h^t\}_{t=1}^{N_f}$ and $\{\mathbf{F}_l^t\}_{t=1}^{N_f}$ are obtained by two time series of adjustable vectors $\{\mathbf{p}_h^t\}_{t=1}^{N_f}$ and $\{\mathbf{p}_l^t\}_{t=1}^{N_f}$ whose elements are evenly-spaced sampled over the intervals $[p_h^1, p_{max} \cdot \mathbf{I}]$ and $[p_l^1, p_{max} \cdot \mathbf{I}]$ respectively. Then, the two time series of feature components are decentralized and transformed by the Inverse Fast Fourier Transform (IFFT): $\{\mathbf{X}_h^t = \mathcal{F}^{-1}(\mathbf{Z}_h^t)\}_{t=1}^{N_f}$, $\{\mathbf{X}_l^t = \mathcal{F}^{-1}(\mathbf{Z}_l^t)\}_{t=1}^{N_f}$. Thus, we obtain two time series of feature components $\{\mathbf{X}_h^t\}_{t=1}^{N_f}$ and $\{\mathbf{X}_l^t\}_{t=1}^{N_f}$ at various high- and low-frequency bands respectively.

3.1.3 Complementary Temporal Aggregation Module

The complementary temporal aggregation module is designed to aggregate the time series of high-frequency components and the time series of low-frequency components obtained from the FVF module, and output a discriminative feature, as shown in the green box in Fig. 1.

Considering that the LSTMs have shown their priority in time-series data modeling, we use LSTMs to model the temporal dependence of the discriminative feature on the multi-band components in this module. Specifically, we use two LSTMs for handling the high-frequency time series $\{\mathbf{X}_h^t\}_{t=1}^{N_f}$ and the low-frequency time series $\{\mathbf{X}_l^t\}_{t=1}^{N_f}$ respectively, each of which provides complementary frequency information for the other one. At the t -th moment ($t \in \{1, 2, \dots, N_f\}$), the

Hidden and Cell states are updated by:

$$\mathbf{H}_h^t = \text{LSTM}_h(\mathbf{H}_h^{t-1}, \mathbf{C}_h^{t-1}, \mathbf{X}_h^t), \quad (5)$$

$$\mathbf{H}_l^t = \text{LSTM}_l(\mathbf{H}_l^{t-1}, \mathbf{C}_l^{t-1}, \mathbf{X}_l^t) \quad (6)$$

where \mathbf{H}_h^t and \mathbf{H}_l^t represent the Hidden states, \mathbf{C}_h^t and \mathbf{C}_l^t represent the Cell states at the t -th moment; \mathbf{X}_h^t and \mathbf{X}_l^t represent the t -th element of the time series $\{\mathbf{X}_h^t\}_{t=1}^{N_f}$ and $\{\mathbf{X}_l^t\}_{t=1}^{N_f}$, respectively. Finally, a discriminative feature \mathbf{X}' can be obtained by concatenating the two updated Hidden states at the N_f -th moment along the channel dimension: $\mathbf{X}' = [\mathbf{H}_h^{N_f}; \mathbf{H}_l^{N_f}]$.

B. CFAN-OSFGR

Here, we introduce the CFAN-OSFGR method for handling the OSFGR task. The CFAN is firstly integrated with a LayerNorm layer for normalization, an average pooling layer for dimension reduction, and a linear classifier for recognition, as shown in Fig. 1. Then, the training strategy and the inference strategy are described as follows.

Training. The model is trained with a cross-entropy classification loss:

$$\mathcal{L}_{cls} = -\frac{1}{N_b} \sum_{k=1}^{N_b} \log p_k \quad (7)$$

where N_b represents the batch size, and p_k represents the probability of the k -th image in the current batch corresponding to the ground-truth class.

Inference. The score outputted from the classifier of the proposed model is used for inference, which is defined as:

$$s = \max_c \{y_c\}, \quad c \in \{1, 2, \dots, C\} \quad (8)$$

where C is the number of the known classes, y_c indicates the c -th ($c \in \{1, 2, \dots, C\}$) element of the logit vector outputted from the classifier corresponding to the c -th class. Besides, a threshold θ , which is chosen to make 90% validation images be correctly recognized as known classes, is used for classifying known-class images and identifying unknown-class images by comparing with the score s :

$$\text{prediction} = \begin{cases} \arg\max_{c \in \{1, 2, \dots, C\}} y_c, & \text{if } s \geq \theta \\ \text{unknown classes}, & \text{if } s < \theta \end{cases} \quad (9)$$

IV. EXPERIMENTS

A. Datasets and Metrics

Datasets. The proposed CFAN-OSFGR method is evaluated on 3 fine-grained datasets (including Aircraft [28], CUB [47], and Stanford-Cars [48]) and 2 coarse-grained datasets which are relatively difficult in the OSR task (including CIFAR+10/+50 [49, 50] and TinyImageNet [51]) under two dataset settings:

(1) *Standard-Dataset Setting.* Under this setting, the known-class and unknown-class images are from the same dataset. Aircraft [28] contains 100-class aircraft images with attributes, 50 classes of which are selected as the known classes. The rest classes are further divided into three modes: ‘Easy’, ‘Medium’, and ‘Hard’ according to their attribute similarity

to the known classes, and we follow the 20/17/13 splitting manner for splitting the unknown classes as done in [23]. CUB [47] contains 200-class bird images with attributes, 100 classes of which are selected as the known classes, and we follow the 32/34/34 splitting manner for splitting the unknown classes as done in [23]. Stanford-Cars [48] contains 196-class car images, the first 98 classes of which are selected as the known classes while the rest 98 classes are used as the unknown classes. In CIFAR+10/+50, 10 classes in CIFAR10 [49] are used as the known classes, while 10 or 50 non-overlapping classes in CIFAR100 [50] are used as the unknown classes. TinyImageNet [51] contains 200-class natural images, 20 classes of which are used as the known classes, while the rest 180 classes are used as the unknown classes.

(2) *Cross-Dataset Setting*. This setting is configured by using the 50 split known classes in Aircraft as the known classes while using all of the 200- and 196-class testing images in CUB and Aircraft as the unknown-class images, respectively.

Metrics. The following evaluation metrics are used under the above dataset settings:

(1) *Standard-Dataset Setting*. On the coarse-grained datasets, we use two metrics for evaluation as done in [8, 14, 17, 20, 21]: (i) AUROC which measures the open-set detection performance by regarding the OSFGR task as a binary classification task (*i.e.*, classification between known classes and unknown classes), and (ii) ACC (*i.e.*, the top-1 accuracy that is widely used in the closed-set classification task) which measures the closed-set classification performance. On the fine-grained datasets, in addition to AUROC and ACC, we also use OSCR (*i.e.*, the open-set classification rate [52]), which is a threshold-independent metric that simultaneously measures the open-set detection performance and the closed-set classification performance, as done in [23].

(2) *Cross-Dataset Setting*. As done in [17, 21, 22], we use macro-F1 score which is a threshold-dependent metric that measures the open-set classification performance by taking the unknown classes as the $(C + 1)$ -th class.

B. Implementation Details

The images from Aircraft and CUB are resized to 448×448 as done in [23], while those from Stanford-Cars are resized to 224×224 . The ResNet50 and the ‘base’ version of Swin Transformer (*i.e.*, SwinB [30]) are used as the feature extractor respectively in the feature extraction module. We use an SGD optimizer with the learning rate of 3×10^{-4} and the weight decay of 1×10^{-4} , as well as an AdamW optimizer [53] with the learning rate of 5×10^{-5} and the weight decay of 0.01 for optimizing the CNN part and the transformer part, respectively. N_t , N_f , N_b and N_c are set to 20, 4, 32, and 128, respectively; p_{min} is set to 0.2 for avoiding filter values being too small, and p_{max} is set to 20 for avoiding the numerical overflow. The originally extracted features are 4-times upsampled for obtaining the preliminary features, and the channels are simultaneously 8-times pruned for decreasing the model complexity. At the inference stage, the values in p_h^1

and p_l^1 are simply set to 1, since the model has been trained to be robust to the variance of these values, as shown in our additional experiments in the supplementary material.

C. Evaluation

4.3.1 Evaluation on the Fine-Grained Datasets

Evaluation Under the Standard-Dataset Setting. Considering that only a few works (CAMV [22] and Cross-Entropy+ [23]) are specially designed for handling the OSFGR task, we also compare the proposed CFAN-OSFGR method with 7 state-of-the-art OSR methods (OpenHybrid [8], OpenGAN [17], ARPL [14], GCPL [13], GMVAE-OSR [10], MoEP-AE-OSR [21] and Trans-AUG [20]). In addition, considering the SwinB-based methods are few, we evaluate one relatively better OSFGR method (Cross-Entropy+) and two relatively better OSR methods (OpenHybrid and ARPL) by replacing their original backbones with SwinB for further comparison.

Tables II, III, and IV report the evaluation results under the *standard-dataset setting* on Aircraft, CUB and Stanford-Cars, respectively. Table V reports the computational resources of these methods on Aircraft. Two points can be seen from these tables:

(1) Transformer-based models achieve better results than CNN-based models in most cases, except in a few cases (*e.g.* on Aircraft) where CNN-based models perform slightly better than transformer-based models. The main reason is that the multiple self-attention operations in transformers boost the model discriminability. Besides, transformer-based models are generally slower than CNN-based models, because the calculations and parameters of fully-connected layers in transformers are generally larger than those of convolutional layers in CNNs.

(2) CFAN-OSFGR outperforms all the comparative methods with the same CNN or SwinB backbone in most cases. We need to point out that CFAN-OSFGR is relatively slower than other methods with the same backbone, mainly due to the feature transformation in the frequency domain as well as the temporal feature aggregation. Furthermore, we conduct an experiment for evaluating the OSFGR performance of different models with similar calculations and parameters, whose results show that CFAN-OSFGR still outperforms other models with similar overheads, the details can be found in the supplementary material.

Evaluation Under the Cross-Dataset Setting. The above results have demonstrated the effectiveness of the proposed CFAN-OSFGR method in cases where known-class images and unknown-class images are from the same dataset. Here, we also evaluate the model performance under the *cross-dataset setting* where the unknown-class images are from outlier datasets. Specifically, the model is trained with Aircraft, and tested with images from CUB and Stanford-Cars as the unknown-class images respectively, whose evaluation results are reported in Table VI. As seen from this table, CFAN-OSFGR outperforms all the other methods significantly in most cases, demonstrating its cross-dataset generalization ability.

4.3.2 Evaluation on the Coarse-Grained Datasets

TABLE II: Comparison of ACC, AUROC, and OSCR results under the *standard-dataset setting* on Aircraft.

Backbone	Method	ACC	AUROC (Easy/Medium/Hard)	OSCR (Easy/Medium/Hard)
CNN	OpenHybrid [8]	0.735	0.884/0.844/0.780	0.718/0.687/0.629
	OpenGAN [17]	0.807	0.841/0.821/0.688	0.795/0.754/0.651
	ARPL [14]	0.917	0.867/0.852/0.674	0.814/0.820/0.657
	GCPL [13]	0.823	0.837/0.828/0.709	0.805/0.761/0.652
	GMVAE-OSR [10]	0.814	0.849/0.833/0.687	0.799/0.753/0.661
	CAMV [22]	0.868	0.880/0.844/0.730	0.801/0.772/0.680
	Cross-Entropy+ [23]	0.917	0.907/0.864/0.776	0.868/0.831/0.754
	CFAN-OSFGR	0.918	0.922/0.873/0.784	0.873/0.847/0.771
SwinB	Backbone	0.896	0.848/0.827/0.723	0.799/0.778/0.686
	OpenHybrid	0.901	0.889/0.830/0.733	0.823/0.781/0.689
	ARPL	0.915	0.880/0.833/0.720	0.836/0.793/0.691
	Cross-Entropy+	0.903	0.859/0.841/0.712	0.814/0.796/0.681
	Trans-AUG [20]	0.898	0.873/0.842/0.739	0.814/0.787/0.689
	MoEP-AE-OSR [21]	0.894	0.907/0.876/0.752	0.831/0.805/0.701
	CFAN-OSFGR	0.917	0.913/0.892/0.839	0.864/0.845/0.803

TABLE III: Comparison of ACC, AUROC, and OSCR results under the *standard-dataset setting* on CUB.

Backbone	Method	ACC	AUROC (Easy/Medium/Hard)	OSCR (Easy/Medium/Hard)
CNN	OpenHybrid [8]	0.683	0.873/0.862/0.739	0.662/0.649/0.531
	OpenGAN [17]	0.799	0.801/0.765/0.707	0.725/0.706/0.648
	ARPL [14]	0.863	0.814/0.772/0.703	0.747/0.710/0.659
	GCPL [13]	0.783	0.805/0.732/0.645	0.711/0.619/0.565
	GMVAE-OSR [10]	0.725	0.826/0.750/0.704	0.694/0.628/0.553
	CAMV [22]	0.836	0.845/0.802/0.709	0.746/0.715/0.640
	Cross-Entropy+ [23]	0.862	0.883/0.823/0.763	0.798/0.754/0.708
	CFAN-OSFGR	0.863	0.883/0.871/0.775	0.803/0.762/0.716
SwinB	Backbone	0.949	0.945/0.875/0.804	0.908/0.848/0.781
	OpenHybrid	0.950	0.953/0.881/0.808	0.918/0.855/0.783
	ARPL	0.952	0.948/0.877/0.810	0.912/0.850/0.788
	Cross-Entropy+	0.953	0.950/0.879/0.815	0.917/0.854/0.794
	Trans-AUG [20]	0.950	0.953/0.882/0.818	0.914/0.854/0.795
	MoEP-AE-OSR [21]	0.948	0.957/0.889/0.814	0.915/0.856/0.787
	CFAN-OSFGR	0.950	0.959/0.899/0.828	0.921/0.870/0.806

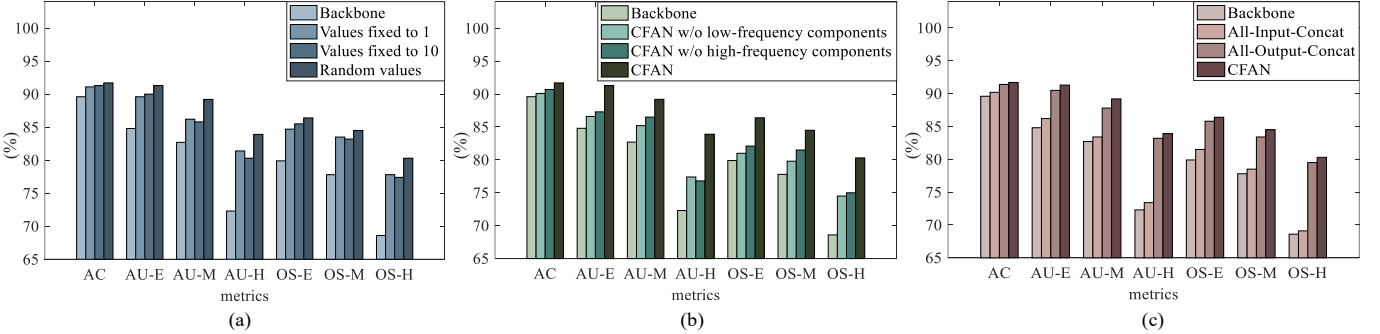


Fig. 3: OSFGR results on Aircraft for analyzing the influence of: (a) randomizing the values in the adjustable vectors p_h^1 and p_l^1 in the FVF module at the training stage; (b) aggregating both high- and low-frequency components in the CTA module; (c) temporal aggregation in the CTA module. The three metrics, ACC, AUROC, and OSCR, are denoted as ‘AC’, ‘AU’, and ‘OS’, respectively. The three difficulty modes, ‘Easy’, ‘Medium’, and ‘Hard’, are abbreviated to ‘E’, ‘M’, and ‘H’, respectively.

The above results have demonstrated the effectiveness of the proposed CFAN-OSFGR method in handling open-set fine-grained images. Here, we further conduct an experiment for evaluating the effectiveness of CFAN-OSFGR in dealing with open-set coarse-grained images. Table VII reports the evaluation results on the two coarse-grained datasets (CIFAR+10/+50 and TinyImageNet). As seen from this table, CFAN-OSFGR still achieves the best results in most cases or achieves the 2nd place. These results further demonstrate that in an open-set scenario, CFAN-OSFGR can not only effectively recognize fine-grained images, but also recognize coarse-grained images accurately.

4.3.3 Evaluation on HFI/LFI

We also evaluate the OSFGR performance of CFAN-OSFGR on HFI/LFI from Aircraft, whose results are reported

in Table I. As seen from this table, CFAN-OSFGR boosts the model performance on both HFI and LFI, indicating that CFAN-OSFGR has better captured both high- and low-frequency information than both ResNet50 and SwinB.

D. Ablation Studies

Here, we conduct extensive ablation studies for evaluating the effectiveness of CFAN-OSFGR more comprehensively. The following experiments are all implemented on Aircraft [28] under the *standard-dataset setting*, and are implemented on SwinB-based CFAN-OSFGR. The main results are reported and analyzed in the following subsections, and some additional results can be found in the supplementary material due to the limitation of space.

4.4.1 Ablation Study on Modules

TABLE IV: Comparison of ACC, AUROC, and OSCR results under the *standard-dataset setting* on Stanford-Cars.

Backbone	Method	ACC	AUROC	OSCR
CNN	OpenHybrid [8]	0.675	0.699	0.637
	OpenGAN [17]	0.704	0.763	0.682
	ARPL [14]	0.752	0.839	0.726
	GCPL [13]	0.688	0.735	0.663
	GMVAE-OSR [10]	0.683	0.756	0.670
	CAMV [22]	0.754	0.832	0.724
	Cross-Entropy+ [23]	0.768	0.859	0.735
CFAN-OSFGR		0.772	0.860	0.754
SwinB	Backbone	0.856	0.905	0.800
	OpenHybrid	0.857	0.910	0.805
	ARPL	0.860	0.908	0.807
	Cross-Entropy+	0.864	0.906	0.808
	Trans-AUG [20]	0.860	0.910	0.809
	MoEP-AE-OSR [21]	0.869	0.922	0.819
CFAN-OSFGR		0.895	0.939	0.859

TABLE V: Computational resources on Aircraft.

Backbone	Method	FLOPs	Params	FPS
CNN	OpenHybrid [8]	32.5G	33.6M	24
	OpenGAN [17]	29.3G	29.1M	35
	ARPL [14]	22.1G	24.0M	41
	GCPL [13]	21.6G	23.8M	42
	GMVAE-OSR [10]	25.2G	32.1M	39
	CAMV [22]	20.7G	23.6M	47
	Cross-Entropy+ [23]	20.8G	23.6M	46
CFAN-OSFGR		42.7G	28.1M	13
SwinB	Backbone	60.6G	86.8M	29
	OpenHybrid	89.9G	98.5M	13
	ARPL	65.3G	87.0M	24
	Cross-Entropy+	60.7G	86.8M	28
	Trans-AUG [20]	60.8G	86.8M	27
	MoEP-AE-OSR [21]	62.8G	91.6M	23
CFAN-OSFGR		86.1G	90.3M	12

Firstly, we conduct an ablation study for analyzing the effect of the last two modules (*i.e.*, the frequency-varying filtering (FVF) module and the complementary temporal aggregation (CTA) module) in the proposed CFAN. The corresponding results are reported in Table VIII. As seen from this table, the model performance improves with the two modules added to the model one by one, indicating that either of the two modules plays an important role in CFAN.

4.4.2 Analysis of the FVF Module

Influence of Randomizing the Values in the Initial Adjustable Vectors in Training. Here, we analyze the influence of randomizing the values in p_h^1 and p_l^1 in the FVF module at the training stage, which converts the high- and low-frequency time series from static time series to dynamic ones at each iteration. Specifically, we train two additional models based on the proposed CFAN-OSFGR method where the values in p_h^1 and p_l^1 are fixed to 1 and 10 respectively, and the corresponding results are shown in Fig. 3 (a). As shown in Fig. 3 (a), the model trained with randomization performs better than the model trained without randomization, demonstrating that the dynamic time series are more effective than the static ones.

4.4.3 Analysis of the CTA Module

Influence of Aggregating High- and Low-Frequency Components. Here, we analyze the influence of aggregating the two time series of components (*i.e.*, the time series of high-frequency components and the time series of low-frequency components) in the CTA module. Specifically, we train two additional models based on CFAN-OSFGR where the dis-

TABLE VI: Comparison of the macro-F1 scores under the *cross-dataset setting*. Under this setting, Aircraft is used as the known-class dataset, while CUB and Stanford-Cars are used as the unknown-class datasets respectively.

Backbone	Method	CUB	Stanford-Cars
CNN	OpenHybrid [8]	0.473	0.840
	OpenGAN [17]	0.426	0.819
	ARPL [14]	0.469	0.831
	GCPL [13]	0.435	0.812
	GMVAE-OSR [10]	0.454	0.826
	CAMV [22]	0.461	0.833
	Cross-Entropy+ [23]	0.482	0.869
CFAN-OSFGR		0.491	0.878
SwinB	Backbone	0.497	0.886
	OpenHybrid	0.499	0.875
	ARPL	0.521	0.888
	Cross-Entropy+	0.503	0.891
	Trans-AUG [20]	0.508	0.882
	MoEP-AE-OSR [21]	0.529	0.876
CFAN-OSFGR		0.546	0.893

TABLE VII: Comparison of AUROC and ACC results on the coarse-grained datasets.

Backbone	Method	CIFAR+10/+50		TinyImageNet	
		ACC	AUROC	ACC	AUROC
CNN	OpenHybrid	0.937	0.962/0.955	0.632	0.793
	OpenGAN	0.940	0.981/0.983	0.684	0.907
	ARPL	0.940	0.965/0.943	0.638	0.762
	GCPL	0.945	0.951/0.946	0.643	0.759
	GMVAE-OSR	0.952	0.952/0.947	0.729	0.782
	CAMV	0.942	0.942/0.933	0.796	0.805
	Cross-Entropy+	0.958	0.954/0.939	0.862	0.826
CFAN-OSFGR		0.961	0.967/0.959	0.865	0.881
SwinB	Backbone	0.981	0.959/0.963	0.904	0.909
	OpenHybrid	0.981	0.978/0.980	0.925	0.934
	ARPL	0.983	0.980/0.985	0.929	0.927
	Cross-Entropy+	0.984	0.965/0.971	0.913	0.916
	Trans-AUG	0.983	0.982/0.986	0.947	0.942
	MoEP-AE-OSR	0.983	0.976/0.975	0.965	0.952
CFAN-OSFGR		0.990	0.994/0.991	0.963	0.955

criminative feature is obtained only from the high-frequency components by $LSTM_h$ or the low-frequency components by $LSTM_l$, whose results are shown in Fig. 3 (b). As shown in Fig. 3 (b), either the high- or the low-frequency component boosts the model performance to some extent but not significantly, and aggregating both time series provides significant performance improvements in most cases, especially under the AUROC and OSCR metrics. These results demonstrate the effectiveness of aggregating both high- and low-frequency information in boosting the generalization ability of the model.

Influence of Temporal Aggregation. Moreover, we analyze the influence of temporal aggregation in the CTA module. Specifically, we compare the proposed temporal aggregation with other two aggregation strategies: (i) concatenating the $2 \cdot N_f$ input feature components in the two time series (denoted as ‘All-Input-Concat’), and (ii) concatenating the $2 \cdot N_f$ Hidden states at all moments (denoted as ‘All-Output-Concat’), whose results are shown in Fig. 3 (c). As shown in Fig. 3 (c), ‘All-Input-Concat’ slightly improves the backbone model performance since it also aggregates high- and low-frequency information, but is inferior to either ‘All-Output-Concat’ or CFAN. Besides, the results of ‘All-Output-Concat’ are slightly lower than those of CFAN since aggregating the Hidden states at earlier moments weakens the effect of temporal modeling. All these results demonstrate the effectiveness of the temporal aggregation strategy, which also provides an enlightening

TABLE VIII: Ablation results on Aircraft by the proposed CFAN-OSFGR method with different configurations of the three modules.

Backbone	FVF module	CTA module	ACC	AUROC (Easy/Medium/Hard)	OSCR (Easy/Medium/Hard)
✓	✗	✗	0.896	0.848/0.827/0.723	0.799/0.778/0.686
✓✓	✓✓	✗	0.913	0.885/0.879/0.824	0.843/0.827/0.781
✓✓	✓✓	✓	0.917	0.913/0.892/0.839	0.864/0.845/0.803

insight into modeling the temporal dependence of an image feature for boosting the feature discriminability.

In addition, we also analyze the influence of p_h^1 and p_l^1 on evaluation, the influence of the number of high/low-pass filters N_f in the FVF module, and the influence of the number of template filters N_t in the FVF module, which can be found in the supplementary material.

V. CONCLUSION

In this paper, we propose the complementary frequency-varying awareness network, CFAN, which learns discriminative features that could effectively capture and make use of both high- and low-frequency feature information from fine-grained images via three sequential modules: the feature extraction module, the frequency-varying filtering module where the frequency-adjustable filter is explored, and the complementary temporal aggregation module. Furthermore, the CFAN-OSFGR method is introduced for handling the open-set fine-grained image recognition task based on the proposed CFAN. Extensive experimental results demonstrate the effectiveness of CFAN-OSFGR.

REFERENCES

- [1] A. Bendale and T. E. Boulton, "Towards open set deep networks," in *IEEE Conference on Computer Vision and Pattern Recognition*, 2016.
- [2] D.-W. Zhou, H.-J. Ye, and D.-C. Zhan, "Learning placeholders for open-set recognition," in *IEEE Conference on Computer Vision and Pattern Recognition*, 2021.
- [3] R. Yoshihashi, W. Shao, R. Kawakami, S. You, M. Iida, and T. Naemura, "Classification-reconstruction learning for open-set recognition," in *IEEE Conference on Computer Vision and Pattern Recognition*, 2019.
- [4] P. Oza and V. M. Patel, "C2ae: Class conditioned autoencoder for open-set recognition," in *IEEE Conference on Computer Vision and Pattern Recognition*, 2019.
- [5] P. Perera, V. I. Morariu, R. Jain, V. Manjunatha, C. Wigginton, V. Ordonez, and V. M. Patel, "Generative discriminative feature representations for open-set recognition," in *IEEE Conference on Computer Vision and Pattern Recognition*, 2020.
- [6] G. Chen, L. Qiao, Y. Shi, P. Peng, J. Li, T. Huang, S. Pu, and Y. Tian, "Learning open set network with discriminative reciprocal points," in *European Conference on Computer Vision*, 2020.
- [7] J. Lu, Y. Xu, H. Li, Z. Cheng, and Y. Niu, "Pmal: Open set recognition via robust prototype mining," in *AAAI Conference on Artificial Intelligence*, 2022.
- [8] H. Zhang, A. Li, J. Guo, and Y. Guo, "Hybrid models for open set recognition," in *European Conference on Computer Vision*, 2020.
- [9] X. Sun, Z. Yang, C. Zhang, K.-V. Ling, and G. Peng, "Conditional gaussian distribution learning for open set recognition," in *IEEE Conference on Computer Vision and Pattern Recognition*, 2020.
- [10] A. Cao, Y. Luo, and D. Klabjan, "Open-set recognition with gaussian mixture variational autoencoders," in *AAAI Conference on Artificial Intelligence*, 2021.
- [11] Y. Guo, G. Camporese, W. Yang, A. Sperduti, and L. Ballan, "Conditional variational capsule network for open set recognition," in *IEEE International Conference on Computer Vision*, 2021.
- [12] H. Huang, Y. Wang, Q. Hu, and M.-M. Cheng, "Class-specific semantic reconstruction for open set recognition," *IEEE Transactions on Pattern Analysis and Machine Intelligence*, 2022, doi:10.1109/TPAMI.2022.3200384.
- [13] H. Yang, X. Zhang, F. Yin, and C. Liu, "Robust classification with convolutional prototype learning," in *IEEE Conference on Computer Vision and Pattern Recognition*, 2018.
- [14] G. Chen, P. Peng, X. Wang, and Y. Tian, "Adversarial reciprocal points learning for open set recognition," *IEEE Transactions on Pattern Analysis and Machine Intelligence*, 2021.
- [15] Z. Ge, S. Demyanov, and R. Garnavi, "Generative openmax for multi-class open set classification," in *British Machine Vision Conference*, 2017.
- [16] L. Neal, M. Olson, X. Fern, W.-K. Wong, and F. Li, "Open set learning with counterfactual images," in *European Conference on Computer Vision*, 2018.
- [17] S. Kong and D. Ramanan, "Opengan: Open-set recognition via open data generation," in *European Conference on Computer Vision*, 2021.
- [18] W. Cho and J. Choo, "Towards accurate open-set recognition via background-class regularization," in *European Conference on Computer Vision*, 2022.
- [19] W. Moon, J. Park, H. S. Seong, C.-H. Cho, and J.-P. Heo, "Difficulty-aware simulator for open set recognition," in *European Conference on Computer Vision*, 2022.
- [20] M. Azizmalayeri and M. H. Rohban, "Ood augmentation may be at odds with open-set recognition," *arXiv preprint. arXiv:2206.04242*, 2022.
- [21] J. Sun, H. Wang, and Q. Dong, "MoEP-AE: Autoencoding Mixtures of Exponential Power Distributions for Open-Set Recognition," *IEEE TCSVT*, 2022, doi:10.1109/TCSVT.2022.3200112.
- [22] W. Dai, W. Diao, X. Sun, Y. Zhang, L. Zhao, J. Li, and K. Fu, "Camv: Class activation mapping value towards open set fine-grained recognition," *IEEE Access*, vol. 9, pp. 8167–8177, 2021.
- [23] S. Vaze, K. Han, A. Vedaldi, and A. Zisserman, "Open-set recognition: a good closed-set classifier is all you need?" in *International Conference on Learning Representations*, 2022.
- [24] N. Park and S. Kim, "How do vision transformers work?" in *International Conference on Learning Representations*, 2022.
- [25] H. Wang, X. Wu, Z. Huang, and E. P. Xing, "High-frequency component helps explain the generalization of convolutional neural networks," in *IEEE Conference on Computer Vision and Pattern Recognition*, 2020.
- [26] R. Geirhos, P. Rubisch, C. Michaelis, M. Bethge, F. A. Wichmann, and W. Brendel, "Imagenet-trained cnns are biased towards texture; increasing shape bias improves accuracy and robustness," in *International Conference on Learning Representations*, 2018.
- [27] W. Brendel and M. Bethge, "Approximating cnns with bag-of-local-features models works surprisingly well on imagenet," in *International Conference on Learning Representations*, 2019.
- [28] S. Maji, E. Rahtu, J. Kannala, M. Blaschko, and A. Vedaldi, "Fine-grained visual classification of aircraft," *arXiv preprint. arXiv:1306.5151*, 2013.
- [29] K. He, X. Zhang, S. Ren, and J. Sun, "Deep residual learning for image recognition," in *IEEE Conference on Computer Vision and Pattern Recognition*, 2016.

- [30] Z. Liu, Y. Lin, Y. Cao, H. Hu, Y. Wei, Z. Zhang, S. Lin, and B. Guo, "Swin transformer: Hierarchical vision transformer using shifted windows," in *IEEE International Conference on Computer Vision*, 2021.
- [31] C. Si, W. Chen, W. Wang, L. Wang, and T. Tan, "An attention enhanced graph convolutional lstm network for skeleton-based action recognition," in *IEEE Conference on Computer Vision and Pattern Recognition*, 2019.
- [32] P. Zhang, W. Ouyang, P. Zhang, J. Xue, and N. Zheng, "Sr-lstm: State refinement for lstm towards pedestrian trajectory prediction," in *IEEE Conference on Computer Vision and Pattern Recognition*, 2019.
- [33] C. Kim, F. Li, and J. M. Rehg, "Multi-object tracking with neural gating using bilinear lstm," in *European Conference on Computer Vision*, 2018.
- [34] L. Zhang, G. Zhu, L. Mei, P. Shen, S. A. A. Shah, and M. Bennamoun, "Attention in convolutional lstm for gesture recognition," in *Conference and Workshop on Neural Information Processing Systems*, 2018.
- [35] R. T. Q. Chen, J. Behrmann, D. K. Duvenaud, and J.-H. Jacobsen, "Residual flows for invertible generative modeling," in *Conference and Workshop on Neural Information Processing Systems*, 2019.
- [36] K. Simonyan and A. Zisserman, "Very deep convolutional networks for large-scale image recognition," *arXiv preprint. arXiv:1409.1556*, 2014.
- [37] N. Dilokthanakul, P. A. Mediano, M. Garnelo, M. C. Lee, H. Salimbeni, K. Arulkumaran, and M. Shanahan, "Deep unsupervised clustering with gaussian mixture variational autoencoders," *arXiv preprint. arXiv:1611.02648*, 2016.
- [38] A. Dosovitskiy, L. Beyer, A. Kolesnikov, D. Weissenborn, X. Zhai, T. Unterthiner, M. Dehghani, M. Minderer, G. Heigold, S. Gelly, J. Uszkoreit, and N. Houlsby, "An image is worth 16x16 words: Transformers for image recognition at scale," *arXiv preprint. arXiv:2010.11929*, 2020.
- [39] K. Han, A. Xiao, E. Wu, J. Guo, C. Xu, and Y. Wang, "Transformer in transformer," in *Conference and Workshop on Neural Information Processing Systems*, 2021.
- [40] W. Wang, E. Xie, X. Li, D. Fan, K. Song, D. Liang, T. Lu, P. Luo, and L. Shao, "Pyramid vision transformer: A versatile backbone for dense prediction without convolutions," in *IEEE International Conference on Computer Vision*, 2021.
- [41] Y. Rao, W. Zhao, Z. Zhu, J. Lu, and J. Zhou, "Global filter networks for image classification," in *Conference and Workshop on Neural Information Processing Systems*, 2021.
- [42] Y. Liu, R. Yu, J. Wang, X. Zhao, Y. Wang, Y. Tang, and Y. Yang, "Global spectral filter memory network for video object segmentation," in *European Conference on Computer Vision*, 2022.
- [43] Z. Qin, P. Zhang, F. Wu, and X. Li, "Fcanet: Frequency channel attention networks," in *IEEE International Conference on Computer Vision*, 2021.
- [44] C. Kleiber and S. Kotza, *Statistical Size Distributions in Economics and Actuarial Sciences*. John Wiley & Sons, 2003.
- [45] G. Agró, "Maximum likelihood estimation for the exponential power function parameters," *Communications in Statistics-Simulation and Computation*, vol. 24, no. 2, pp. 523–536, 1995.
- [46] R. D. Luce, "Reduction invariance and prelec's weighting functions," *Journal of Mathematical Psychology*, vol. 45, no. 1, pp. 167–179, 2001.
- [47] C. Wah, S. Branson, P. Welinder, P. Perona, and S. Belongie, "The CaltechUCSD Birds-200-2011 Dataset," California Institute of Technology, Tech. Rep., 2011.
- [48] J. Krause, M. Stark, J. Deng, and L. Fei-Fei, "3d object representations for fine-grained categorization," in *IEEE International Conference on Computer Vision*, 2013.
- [49] A. Krizhevsky and G. Hinton, "Convolutional deep belief networks on cifar-10," 2010, *Technical report*.
- [50] A. Krizhevsky, "Learning multiple layers of features from tiny images," 2009, *Technical report*.
- [51] Y. Le and X. Yang, "Tiny imagenet visual recognition challenge," 2015, *CS 231N*.
- [52] A. R. Dhamija, M. Günther, and T. E. Boulton, "Reducing network agnostophobia," in *Conference and Workshop on Neural Information Processing Systems*, 2018.
- [53] I. Loshchilov and F. Hutter, "Fixing weight decay regularization in adam," in *International Conference on Learning Representations*, 2018.